Carbon Coating, Carburization and High Temperature Stability Improvement of Cobalt Nanorods

Mona Ibrahim, Cécile Marcelot, Kahina Aït-Atmane, Ekrame Berrichi,
Lise-Marie Lacroix, Antoine Zwick, Bénédicte Warot-Fonrose, Sébastien
Lachaize, Philippe Decorse, Jean-Yves Piquemal, et al.

HAL Id: hal-00912966
https://hal.science/hal-00912966

Carbon Coating, Carburization and High Temperature Stability Improvement of Cobalt Nanorods

Mona Ibrahim, [a] Cécile Garcia,[a] Kahina Aït Atmane,[b] Ekrame Berrichi,[b] Lise-Marie Lacroix,[a] Antoine Zwick,[c] Bénédicte Warot-Fonrose,[c] Sébastien Lachaize,[a] Philippe Decorse,[b] Jean-Yves Piquemal[b] and Guillaume Viau[a,*]

[a] Université de Toulouse, LPCNO, INSA CNRS UMR 5215, 135 av. de Rangueil, 31077 Toulouse cedex 4, France

[b] Université Paris Diderot, Sorbonne Paris Cité, ITODYS, UMR CNRS 7086, 15 rue J.-A. de Baïf, 75205 Paris cedex 13, France

[c] CEMES, UPR CNRS 8011, 29, rue Jeanne Marvig, BP 94347, 31055 Toulouse Cedex 4, France

Corresponding author:

Guillaume Viau

INSA Toulouse

* E-mail: gviau@insa-toulouse.fr (G. Viau)

ABSTRACT

The reactivity of highly crystalline hcp cobalt nanorods (NRs) with organic solvents at high temperature was studied. Cobalt NRs with a mean diameter of 15 nm were first synthesized by the polyol process and then heated at 300 °C in octadecene (ODE), oleylamine (OA) or mixtures of these two solvents. The surface and structural modifications of the Co NRs were characterized by Raman spectroscopy, X-ray photoelectron spectroscopy (XPS), X-ray diffraction (XRD) and scanning and transmission electron microscopy (SEM and TEM). A disordered carbon shell was formed at the cobalt rod surface, the thickness of which can be tuned from 5 to 25 nm by increasing the amount of oleylamine in the solvent mixture. This carbon shell partially reduced the native cobalt oxide observed at the surface of the NRs and drastically improved their temperature stability as inferred from in-situ XRD study and TEM. The shape anisotropy and the crystallite anisotropy of the hcp phase are both preserved up to 400 °C for the carbon coated cobalt rods whereas the uncoated NRs lose their anisotropy at 225 °C. Treatments at 300 °C in ODE/OA mixtures for different durations allowed the progressive carburization of Co to Co_2C. The crystallographic orientation of the Co_2C grains within the cobalt NRs combined with the different carbon shell thickness on the $\{10\bar{1}0\}$ and (0001) facets of the rods suggested a preferential carburization from the lateral facets of the hcp cobalt rods.

Introduction

The high saturation magnetization of the metal magnetic nanoparticles (NPs) makes them particularly interesting for several applications. However, Fe, Co and FeCo NPs require, for biomedical applications to increase their stability toward oxidation and to make them biocompatible.[1,2] The growth of a carbon shell can address this issue[3]; it can also strongly improve their thermal stability[4,5] and open wider possibilities such as covalent grafting of organic groups or biomolecules that add new functions to the magnetic particles.[6,7]

Different routes for carbon encapsulated cobalt and iron particles have been described like carbon arc process[3, 8, 9, 10] or chemical vapour deposition.[1,11,12,13,14] In these methods the cobalt precursors were either ultrafine cobalt oxide powder or organometallic precursors, the cobalt particles were formed at high temperature and therefore exhibit a spherical shape and generally the fcc structure. Amorphous cobalt cores surrounded by a carbon shell were produced by laser ablation of a cobalt target immersed in toluene[15] or by decomposition of metallocene powders under a laser beam.[16] Sonochemical decomposition of $Fe(CO)_5$ in high boiling point aromatic solvent[17] and thermal decomposition of iron stearate[18] at 900 °C are other examples of one-pot reaction that produced air stable carbon encapsulated Fe and Fe_3C nanocrystals with high yield. Methods were also developed to coat with a carbon shell monodisperse Co NPs first prepared by wet chemistry. The principle in that case was to carry out a pyrolysis of the organic molecules (surfactants or polymers) anchored at the particle surface. Stable encapsulated cobalt particles were obtained with temperature pyrolysis in the range 700-1000 °C.[19,20] Milder conditions were found using an aqueous solution of glucose that allowed a carbon coating of cobalt nanostructures by a treatment at 160 °C in hydrothermal conditions.[21]

The magnetic nanorods (NRs) and nanowires (NWs) exhibit peculiar properties because of their high magnetic anisotropy. Elongated magnetic objects find applications in composite

materials[22] or as biosensors.[23] Coercivity higher than 6 kOe were measured on cobalt nanorods (NRs) and nanowires (NWs) synthesized by the polyol proces[24] or by organometallic chemistry.[25] Composite materials of well aligned cobalt wires are expected to exhibit high $(BH)_{max}$ values.[26] Nevertheless we showed recently that the thermal stability of the cobalt rods prepared by the polyol process in powder form was limited to 225 °C.[27] Above this temperature the sintering of the rod irreversibly altered their magnetic properties.[27] In situ transmission electron microscopy experiments demonstrated that a controlled encapsulation in a C shell of Ge[28] and Co[4] nanowires at moderate temperatures increased their thermal stability. Following this idea our goal was to develop a simple method to coat cobalt rods prepared by the polyol process with a thin carbon shell in order to improve their thermal stability. All the methods consisting in the decomposition of a carbon precursor requiring high temperature were not suited for the coating of hcp cobalt particles due to the phase transformation of hcp toward fcc occurring at 450 °C.

In this article we examine the possibility to coat cobalt NRs with a carbon shell thanks to the decomposition of high boiling organic solvents at 300 °C and we report on the thermal stability of these carbon coated Co NRs. We show that a carburization of cobalt can occur depending on the experimental conditions and that these nanorods are also model materials to study how C atoms incorporate in the Co hcp structure to form the cobalt carbide Co_2C.

Experimental Methods

Synthesis and coating of Co nanorods

Sodium hydroxide was purchased from VWR, ruthenium chloride hydrate ($RuCl_3$, x H_2O) and 1,2 butanediol from Fluka, cobalt acetate tetra hydrate and octadecene (ODE) from Alfa Aesar, lauric acid and oleylamine (OA) from Acros.

Cobalt nanorods were synthesized by reduction of cobalt laurate in a basic solution of 1,2 butanediol according to a procedure previously published.[24] Cobalt laurate (0.08 M) was dispersed in a sodium hydroxide solution (0.08M) of 1,2 butanediol containing ruthenium chloride (2.10^{-3} M). The suspension was heated up to 175 °C and this temperature was maintained for 30 min after the solution turned to black indicating the cobalt reduction. The cobalt particles were recovered by centrifugation and washed twice with absolute ethanol. The cobalt rods were characterized by X-ray diffraction and electron microscopy.

The cobalt nanorods were dispersed and heated in a high boiling point organic solvent in order to provoke the solvent decomposition at the surface of NRs. Two different solvents were studied: ODE and OA. Suspensions of cobalt rods in ODE, OA, or a mixture of these two solvents were heated at 180 °C for 30 min under a flux of argon to ensure the complete evaporation of ethanol, and then at 300 °C under Ar atmosphere for a time varying between 30 min to 4h. The treated particles were characterized by Raman spectroscopy, X-ray diffraction, electron microscopy and magnetometry.

Characterizations

Raman spectra were obtained at room temperature with a Dilor XY microspectrometer equipped with a 1024×256 pixel thermoelectrically cooled Jobin-Yvon CCD detector using an excitation line at 514.5 nm from a Spectra Physics Model 165 argon ion laser (power: 150 µW). The carbon and hydrogen mass fractions in the samples were determined using a Flash 2000 Organic Elemental Analyzer from Thermo. Transmission electron microscopy (TEM) characterizations were performed using a Jeol 1400 microscope operating at 120 kV. High resolution transmission electron microscopy (HRTEM) images were obtained with a Tecnai F20 (200 kV) instrument equipped with a spherical aberration corrector. Scanning electron microscopy (SEM) was performed using a Zeiss SUPRA 40 FESEM controlled by a

computer workstation. The electron source is a thermal field emission gun (Schottky type). Images are created using the SMARTSEM software. X-Ray Diffraction (XRD) patterns obtained using Co K_α radiation (λ = 1.7889 Å) were recorded on a PANalytical X'Pert Pro diffractometer equipped with an X'celerator detector in the range 20-100 ° with a 0.067 ° step size and 150 s per step. In order to follow the structural evolution of the carbon cobalt nanorods with temperature, in-situ thermal treatments were realized in the range 25-500 °C under a nitrogen atmosphere (N_2 Alphagaz 1 : O_2 < 2 ppm or N_2 Alphagaz 2 : O_2 < 0.1 ppm) using a HTK 1200N high-temperature X-ray diffraction chamber from Anton Paar. The samples were heated inside the high temperature X-ray diffraction chamber from room temperature to the final temperature using a 5 K·min^{-1} rate and maintained for 2 h at the final temperature prior to the acquisition of the X-ray diffraction pattern. X-ray photoelectron spectroscopy (XPS) signals were recorded using a Thermo VG ESCALAB 250 system equipped with a micro-focused, monochromatic Al Kα X-ray source (1486.6 eV) and a magnetic lens which increases the electron acceptance angle and hence the sensitivity. A 650 µm sized X-ray beam was used at a power of 200 W (15 kV). The samples were fixed on sample holder using conductive double-sided tape and outgassed in the fast entry lock chamber at 1×10^{-7} mbar. The spectra were acquired in the constant analyser energy mode, with a pass energy of 100 and 40 eV for the survey and the narrow regions, respectively. Charge compensation was achieved with an electron flood gun for insulating samples. The energy and emission current of the electrons were 4 eV and 0.15 to 0.20 mA, respectively. Avantage software, version 4.67, was used for data digital acquisition and processing. The peak binding energy positions were calibrated by setting the C1s component due to hydrocarbon contamination at 285 eV. Magnetic measurements were performed using a Quantum Design MPMS-5S SQUID magnetometer.

Results and Discussion

A. Carbon coated cobalt nanorods

Chemical analysis revealed that the carbon mass fraction in the cobalt rod samples increased from 3.8% to 23.4% after a chemical treatment of 3h in ODE at 300 °C, while the hydrogen mass fraction increased from 0.85% to 1.5%. The Raman spectra of the cobalt rods heated either in ODE or OA at 300 °C exhibit two bands at 1340 and 1600 cm^{-1} indexed as the D and G bands of a disordered carbon, respectively (Figure 1). The G band corresponds to the sp^2 C while D band is related to the presence of sp^3 C and reveals the presence of structural defaults. The intensity ratio I_D/I_G is a good indicator of the disorder in the carbon layer.[29] In this study the I_D/I_G ratio varies in the range $0.67 - 0.8$ depending on the nature of the organic solvent in which the cobalt rods have been treated, the carbon obtained with the treatment in ODE being less disordered (Figure 1). Note that the D and G bands of the carbon can only be observed on the Raman spectra for a low laser power. For higher laser power, the D and G bands vanish and four bands at 190, 470, 510 and 690 cm^{-1} attributed to Co_3O_4 appear. This is explained by the fact that the carbon coating may be burnt off when irradiated in air with a high laser power. In such case the Raman spectrum of "naked" hence readily oxidized cobalt rods is then retrieved.

The scanning electron microscope images show that the cobalt rods treated in ODE at 300 °C for 3h preserve their anisotropic shape but undergo a surface modification (Figure 2a). The transmission electron microscopy images show a thin carbon shell around the cobalt rods (Figure 2b) with a thickness of about 4 nm. HRTEM images show that this shell exhibits locally an onion structure with a distance in the range 3.4-3.5 Å (Figure 2c).

X-ray photoelectron spectroscopy was performed on cobalt rods treated at 300 °C for 3h in ODE and on the raw cobalt rods as reference. The main peaks observed in the survey scans of the two samples are C 1s, O 1s and Co 2p peaks centered at ca. 285, 530 and 778-800 eV, respectively (Figure 3a). For the treated rods the C 1s peak intensity increases and becomes much higher than the O 1s peak. This can be interpreted by the deposition of a continuous carbon shell around the rods in good agreement with the TEM images. The Co $2p_{3/2}$ and $2p_{1/2}$ high resolution spectra were fitted with three components corresponding to Co(0), Co(II) and the shake-up (satellites) peaks (Figure 3b). Both for the raw Co NRs and for the NRs treated at 300 °C the first peak maximum was found at 778.2 eV which is consistent with the Co $2p_{3/2}$ binding energy of Co in a zerovalent state.[30] The second peak exhibited a maximum at 781.2 eV and 780.6 eV for the raw Co NRs and for the NRs treated at 300 °C, respectively. This peak is attributed to Co in a 2+ valence state in agreement with the Co 2p3/2 binding energy of Co(OH)$_2$ and CoO that are generally given in the ranges 781-782 eV and 780-780.9 eV, respectively.[30] The Co(0)/[Co(0)+Co(II)] surface ratio was determined from the integrated peak areas. This ratio was 6% in the raw Co NRs. The main contribution of the Co(II) is well explained by the existence of a thin CoO layer at the surface of the rods that screens the cobalt metal.[31] In the carbon coated Co NRs the Co(0)/[Co(0)+Co(II)] ratio increased to 17 %. This increasing amount of the Co(0) contribution shows that the chemical reaction at the cobalt surface that leads to a carbon coating also partially reduces the cobalt oxide layer. The small energy shift of the Co(II) contribution from 781.2 eV to 780.6 eV observed with the carbon coating can be interpreted by the elimination of the hydroxyl and carboxylate groups at 300°C in favour of CoO.

It is well established that the cobalt NRs crystallize with the hcp structure with the crystallographic c axis parallel to the long axis of the rods.[24] The zone axis of the cobalt wire in figure 2c is [11$\bar{2}$0] which means that the long axis of the rods is parallel to the [0002]

direction. The crystallite anisotropy is also inferred from the XRD pattern. The two mean crystallite sizes $L_{(10\bar{1}0)}$ and $L_{(0002)}$, calculated from the broadening of the Co hcp $(10\bar{1}0)$ and (0002) lines, respectively, are found much different from each other due to the anisotropy of the crystallite. The mean crystallite size $L_{(10\bar{1}0)}$ is almost the rod diameter showing a good crystallinity in the diameter while the mean crystallite size $L_{(0002)}$ is found much lower than the rod length maybe due to stacking faults as it was already observed in several examples of raw cobalt rods prepared by the polyol process.[24]

The cobalt rod structure remains unchanged with the treatment in pure ODE for 3h, the XRD pattern is indexed as pure cobalt with the hcp structure (Figure 4a). We must note that the line corresponding to the carbon graphite at 3.5Å is not visible on the XRD pattern of the carbon coated Co NRs. This can be explained by a very disordered carbon shell with small crystallites leading to very broad peaks that are not easily detected on the XRD pattern. The mean crystallite sizes $L_{(10\bar{1}0)}$ and $L_{(0002)}$ were found 12 nm and 38 nm, respectively. These values are similar to those measured in the raw Co NRs pattern, showing that the treatment of the cobalt rods at 300 °C in ODE for 3h did not modify the crystallite anisotropy.

B. Transformation to cobalt carbide

Treatments of the cobalt rods at high temperature in ODE/OA mixtures may induce a more dramatic modification of the rod morphology and structure. The XRD patterns of the rods treated in the ODE/OA mixture for different durations are given on Figure 4b-c. These patterns exhibit additional lines attributed to the cobalt carbide Co_2C.[32] The (111) peak of the orthorhombic Co_2C (d_{111} = 2.12 Å ; 2θ = 49.9 °) appears first (Figure 4b). For a longer treatment the (020), (002), and (021) peaks at the distances d_{020} = 2.22 Å (2θ = 47.45 °), d_{002} = 2.185 Å (2θ = 48.3 °) and d_{021} = 1.98 Å (2θ = 53.7 °) are clearly seen on the pattern (Figure 4c). After a treatment of 4h at 300 °C in the ODE/OA mixture, the Co metal lines totally

9

disappeared and the compound consisted in a pure cobalt carbide powder (Figure 4d). It is well known that fine cobalt powders are sensitive to carburization when they are prepared in an organic solvent at high temperature.[33, 34, 35] The carburization of cobalt can give two different carbides, Co_3C and Co_2C.[33] In these experiments Co_3C was never observed: the carburization of the hcp cobalt NRs leading only to Co_2C. Figure 5 presents TEM images of cobalt rods treated in ODE/OA mixtures. The partially carburized cobalt rods obtained after 3h at 300 °C are coated by a thicker carbon layer than in ODE, with a thickness in the range 9-23 nm and a mean value of 16 nm (Figure 5a). The rods still exhibit an anisotropic shape but their surfaces are rough. It is noteworthy that the carbon shell is much thinner at the rod tips (Figure 5a). HRTEM studies of the partially carburized rods treated 3h at 300 °C revealed that the same rod can contain Co_2C grains inserted in the Co hcp phase (Figure 6). The diffraction pattern calculated from the HRTEM image of the Co grain was indexed as the $[11\bar{2}0]$ zone axis of the hcp structure showing that the c axis is parallel to the rod axis. The diffraction pattern calculated from the HRTEM image of the Co_2C grain was indexed as the [100] zone axis of the expected orthorhombic structure (Figure 6). The crystallographic orientation relationships between the carbide and the metal are $[100]Co_2C\|[11\bar{2}0]Co_{hcp}$ and $(001)Co_2C\|(0001)Co_{hcp}$. The angle between the [001] direction of Co_2C and the [0001] direction of the hcp Co is less than 2° showing a very small mismatch. The same crystallographic relationship was reported by Nagakura on Co/Co_xC thin films.[36]

When the Co to Co_2C carburization was complete after an extended treatment, the particles were no longer anisotropic but consisted in isotropic particles with a size in the range 9-25 nm and a mean size of 15 nm (Figure 5b). These particles are organized in chains embedded in a carbonaceous coating. All the chains have more or less the same diameter (40-50 nm) evidencing the initial anisotropic cobalt particles.

C. High temperature properties of carbon coated cobalt nanorods

The high temperature in-situ X-ray diffraction (HT XRD) patterns under a N_2 atmosphere with O_2 concentration < 2 ppm of Co NRs coated with a thin carbon layer showed that the hcp structure is preserved for temperature up to 400 °C (Figure 7a). At 450 °C the hcp to fcc phase transformation occurs as predicted by the phase diagram of bulk cobalt. The formation of the fcc phase is clearly seen with the (200) peak, $d_{200} = 1.77$ Å (2θ = 60.6°). In the temperature range 100-250 °C there is also the growth of the (111) and (200) fcc cobalt oxide CoO lines, $d_{111} = 2.46$ Å (2θ = 42.6°) and $d_{200} = 2.13$ Å (2θ = 49.65°), that corresponds to the crystallization of the native oxide layer. Above 250 °C the CoO lines vanish because of the reduction of the cobalt oxide layer by the carbonaceous matter at the particle surface. No trace of re-oxidation of the Co NRs was observed in the temperature range studied. The behaviour of the non coated Co NRs at high temperature under the same atmosphere was very different. At 250°C the (220) line of Co_3O_4 (d = 2.86 Å, 2θ = 36.5 °) appeared. At 350 °C the pattern is indexed as a mixture of hcp Co, CoO and Co_3O_4 (Figure 7b). Even if the O_2 content in the nitrogen atmosphere is small the non coated rods were irreversibly oxidized above this temperature contrarily to the carbon coated rods.

The mean crystallite sizes $L_{(10\bar{1}0)}$ and $L_{(0002)}$ of the carbon coated Co NRs were calculated using the Scherrer formula and plotted as a function of the annealing temperature (Figure 7c). The $L_{(10\bar{1}0)}$ value is almost constant all over the temperature range 25-400 °C. A small increase is observed at 300 °C concomitant with the CoO elimination. This can be interpreted as the increase of the metal diameter due to the reduction of the native oxide layer. The $L_{(0002)}$ at 400 °C is 36 nm, very close to the RT value (Figure 7c) which means that the anisotropy of the hcp crystallite is retained up to 400 °C. At 450 °C both $L_{(10\bar{1}0)}$ and $L_{(0002)}$ strongly increase showing that the rod morphology is definitively lost due to the phase transition hcp to fcc. The

L$_{(0002)}$ variation in the intermediate range of annealing temperature is more difficult to interpret. L$_{(0002)}$ decreases progressively up to 250 °C and then increases suddenly to reaches at 300 °C the room temperature value (Figure 7c). The minimum of L$_{(0002)}$ corresponds to the maximum of oxidation. The formation of a thicker CoO layer seems to decreases the crystallographic coherence length along the c axis but this decreasing is reversible.

The high temperature in situ X-ray diffraction patterns of the partially carburized Co NRs coated with a thick carbon layer and annealed under a N$_2$ atmosphere (O$_2$ < 0.1 ppm) at different temperatures showed that the cobalt carbide disappears between 300 and 350 °C (Figure 8). The pure hcp structure is retrieved above 350 °C. No evidence of CoO crystallization was found in the intermediate temperature patterns in good agreement with our previous observation that prolonged treatment reduces the cobalt oxide native layer. As in the case of the non carburized rods a textural anisotropy is preserved at 400 °C, inferred from the larger broadening of the $(10\bar{1}0)$ line compared to the (0002) one. Nevertheless, the TEM images showed that the mean aspect ratio decreased after the thermal treatment at 400 °C. This can be interpreted by a morphological modification with the decarburization of the Co$_2$C grains located within the rod.

On the other hand the high aspect ratio of the carbon coated Co NRs free of carbide was preserved for annealing up to at 400 °C for 2h as inferred from TEM images (Figure 9). The room temperature magnetic properties of the carbon coated Co NRs were measured before and after the thermal treatment at 400 °C (Figure 10). In both cases the magnetization curve exhibits a remanence to saturation magnetization ratio of 0.5, the expected value for a powder in which particles are randomly oriented in the applied magnetic field. The coercivity is almost constant, it increases from 3500 Oe to 3600 Oe after thermal treatment. Such coercivity values are in good agreement with the previous ones measured on cobalt rods prepared by the polyol process.[24,27] Indeed, according to the Stoner-Wolfarth model, an

assembly of the same Co NRs perfectly ordered parallel to the applied field should exhibit a coercivity value of 7000 Oe. The high magnetic anisotropy of these rods comes from the addition of shape anisotropy and magnetocrystalline anisotropy. This study shows that the carbon coating and the subsequent annealing at 400 °C do not lower the magnetic anisotropy. The saturation magnetization of the carbon coated Co NRs is 103 emu per gram of powder. This value increases to 117 emu.g^{-1} after annealing at 400 °C for 2h. This increase of 14% corresponds to the loss of organic matter and to the partial reduction of the CoO shell during the annealing process. The saturation magnetization is lower than the bulk cobalt value because an important amount of carbon remains after the annealing.

D. Discussion

This work shows that the decomposition of organic solvents at 300 °C is a simple route to coat cobalt nanorods with a thin carbon shell. The pyrolysis of polymers to produce a carbon coating is generally performed in a gas phase at much higher temperature. In our case, milder conditions were necessary to keep both the hcp structure and the anisotropic shape of the rods. The interest to carry out the carbon coating in a liquid phase is that individual nanorods are coated and remain stabilized in solution: no agglomeration was observed after coating. The 5 nm carbon shell obtained by a treatment in ODE at 300 °C improves the thermal stability of the Co NRs. Indeed the carbon coated Co NRs remain unchanged even after annealing in powder form at 400 °C. This behaviour is very different from the one of raw cobalt NRs. A previous study on the high temperature stability of raw cobalt rods showed that in absence of a carbon coating the anisotropy was lost at 225 °C.[27] At this annealing temperature a strong increase of the mean crystallite sizes $L_{(10\bar{1}0)}$ and $L_{(0002)}$ was observed, the crystallite lose their anisotropy and the TEM revealed a particle sintering. Thus, we can conclude that the thin carbon coating acts as an efficient barrier for the particle sintering at temperature as high as

400 °C and preserves the particle anisotropy. Moreover, in a slightly oxidative atmosphere the carbon layer can act as a sacrificial shell that preserves the cobalt core from oxidation (Figure 7).

It is well established that small organic molecules like carbon monoxide or ethylene can decompose at the surface of Fischer-Tropsch cobalt catalysts at relatively low temperature and form a carbon deposition, being a cause of deactivation.[37] The carbon coating in our case results certainly from a mechanism similar to the carbon deposition on the Fischer-Tropsch cobalt catalysts.

The thickness of the carbon shell can be varied in the range 5-20 nm, but a thick shell comes along with a carburization. Ping Liu *et al.* described the formation of Co_2C nanoparticles in tetra ethylene glycol by a carburization of cobalt particles formed at first in the medium.[34] Our study confirms that the decomposition of organic solvents at the surface of cobalt NRs is a source of carbon atoms that first form a carbon shell at the surface and then diffuse into the metal crystal to form carbide. In this study the carburization of the hcp cobalt NRs leads only to Co_2C. The formation of Co_2C is generally described as the result of the intercalation of C atoms in the hcp ABAB stacking of the (0001) dense planes.[34, 36, 38] The cobalt NRs expose mainly $\{10\bar{1}0\}$ crystallographic facets which is favourable to the C intercalation in the metal array (Figure 11). The crystallographic relationships between the hcp Co grain and the Co_2C grain inserted in the hcp stacking inferred from the HRTEM study (Figure 6) correspond exactly to this mechanism. The difficulty to insert carbon from the (0001) planes and/or a difference in the catalytic activity for the decomposition of the organic molecules of the two different facets can explain why the carbon shell is much thinner at the rod tips than on the sides (Figure 5a). The formation of a thick carbon coating around the cobalt rods seems related to their ability to form a carbide. This observation reminds results reported on the activity of cobalt-based Fischer-Tropsch catalysts.[38] Indeed the higher activity for CO

conversion in Fischer-Tropsch conditions of hcp cobalt was explained by the easiest facility of hcp Co particles to form carbide, the C atoms being extracted by the hydrogen to form hydrocarbon molecules.[38]

Conclusion

A simple and rapid method to encapsulate cobalt nanorods into a thin carbon layer through a thermal treatment in organic solvents at 300 °C has been described. This carbon shell does not modify the magnetic anisotropy of the cobalt rods and strongly improve their thermal stability. The Co@C core shell NRs that have been produced are stable up to 400 °C and are promising building blocks for the elaboration of anisotropic nanomaterials by consolidation experiments. Moreover, the growth of a carbon shell by this method opens the way to a covalent functionalization at the cobalt NRs surface with organic molecules and to the grafting of polymers that will favor the NRs dispersion into a polymeric matrix or to add new functionalities.

This study has also confirmed that the (0001) and the $\{10\bar{1}0\}$ facets of the hcp cobalt exhibit a different reactivity toward the C insertion and points to possible future works on the use of cobalt particles with well defined morphology as model Fischer-Tropsch catalysts.

References

(1) Lukanov, P. ; Anuganti, V. K. ; Krupskaya, Y. ; Galibert, A.-M. ; Soula, B. ; Tilmaciu, C. ; Velders, A. H. ; Klingeler, R. ; Büchner, B. ; Flahaut, E. CCVD Synthesis of Carbon-Encapsulated Cobalt Nanoparticles for Biomedical Applications. *Adv. Funct. Mater.* **2011**, *21*, 3583-3588.

(2) Mehdaoui, B. ; Meffre, A. ; Carrey, J. ; Lachaize, S. ; Lacroix, L. M. ; Gougeon, M.; Chaudret, B. ; Respaud, M. Optimal Size of Nanoparticles for Magnetic Hyperthermia : A Combined Theoretical and Experimental Study. *Adv. Func. Mater.* **2011**, *21*, 4573-4581.

(3) Seo, W. S.; Lee, J. H.; Sun, X.; Suzuki, Y.; Mann, D.; Liu, Z.; Terashima, M.; Yang, P. C.; McConnell, M. V.; Nishimura, D. G.; Dai, H. FeCo/Graphitic-Shell Nanocrystals as Advanced Magnetic-Resonance-Imaging and Near-Infrared Agents. *Nat. Mater.* **2006**, 5, 971-976.

(4) Ciuculescu, D.; Dumestre, F.; Comesana-Hermo, M.; Chaudret, B.; Spasova, M.; Farle, M.; Amiens, C. Single-Crystalline Co Nanowires: Synthesis, Thermal Stability, and Carbon Coating. *Chem. Mater.* **2009**, *21*, 3987-3995.

(5) Rong, C.-B.; Poudyal, N.; Chaubey, G. S.; Nandwana, V.; Liu, Y.; Wu, Y. Q.; Kramer, M. J.; Kozlov, M. E.; Baughman, R. H.; Ping Liu, J. High Thermal Stability of Carbon-Coated $L1_0$-FePt Nanoparticles Prepared by Salt-Matrix Annealing. *J. Appl. Phys.* **2008**, *103*, 07E131.

(6) Tan, C. G.; Grass, R. N. Suzuki Cross-Coupling Reactions on the Surface of Carbon-Coated Cobalt: Expanding the Applicability of Core–Shell Nano-Magnets. *Chem. Commun.* **2008**, 4297-4299.

(7) Fuhrer, R.; Herrmann, I. K.; Athanassiou, E. K.; Grass, R. N.; Stark, W. J. Immobilized β-Cyclodextrin on Surface-Modified Carbon-Coated Cobalt Nanomagnets: Reversible Organic Contaminant Adsorption and Enrichment from Water. *Langmuir* **2011**, *27*, 1924-1929.

(8) McHenry, M. E.; Majetich, S. A.; Hartman, J. O.; DeGraef, M.; Staley, S. W. Superparamagnetism in Carbon-Coated Co Particles Produced by the Kratschmer Carbon Arc Process. *Phys. Rev.* B **1994**, *49*, 11 358-11 363.

(9) Seshadri, R.; Sen, R.; Subbanna, G. N.; Kannan, K. R.; Rao, C. N. R. Iron, Cobalt and Nickel Nanoparticles Encapsulated in Carbon Obtained by the Arc Evaporation of Graphite with the Metals. *Chem. Phys. Lett.* **1994**, *231*, 308-313.

(10) Bonard, J.-M.; Seraphin, S.; Wegrowe, J.-E.; Jiao, J.; Châtelain, A. Varying the Size and Magnetic Properties of Carbon-Encapsulated Cobalt Particles. *Chem. Phys. Lett.* **2001**, *343*, 251-257.

(11) El-Gendy, A. A.; Ibrahim, E. M. M.; Khavrus, V. O.; Krupskaya, Y.; Hampel, S.; Leonhardt, A.; Büchner, B.; Klingeler, R. The Synthesis of Carbon Coated Fe, Co and Ni Nanoparticles and an Examination of their Magnetic Properties. *Carbon* **2009**, *47*, 2821-2828.

(12) Wang, Z. H.; Choi, C. J.; Kim, B. K.; Kim, J. C.; Zhang, Z. D. Characterization and Magnetic Properties of Carbon-Coated Cobalt Nanocapsules Synthesized by the Chemical Vapor-Condensation Process. *Carbon* **2003**, *41*, 1751-1758.

(13) Liu, B. H.; Ding, J.; Zhong, Z. Y.; Dong, Z. L.; White, T.; Lin, J. Y. Large-Scale Preparation of Carbon-Encapsulated Cobalt Nanoparticles by the Catalytic Method. *Chem. Phys. Lett.* **2002**, *358*, 96-102.

(14) Li, H.; Zhao, N.; He, C.; Shi, C.; Du, X.; Li, J. Fabrication of Carbon-Coated Cobalt Nanoparticles by the Catalytic Method. *J. Alloys and Compounds* **2008**, *458,* 130-133.

(15) Kwong, H. Y.; Wong, M. H.; Leung, C. W.; Wong, Y. W.; Wong, K. H. Formation of Core/Shell structured Cobalt/Carbon Nanoparticles by Pulsed Laser Ablation in Toluene. *J. Appl. Phys.* **2010**, *108*, 034304.

(16) Huh, S. H.; Nakajima, A. Laser Synthesis and Magnetism of Amorphous Iron and Cobalt Carbide Nanoparticles with Carbon Onion. *J. Appl. Phys.* **2006**, *99*, 064302.

(17) Nikitenko, S. I.; Koltypin, Y.; Palchik, O.; Felner, I.; Xu, X. N.; Gedanken, A. Synthesis of Highly Magnetic, Air-Stable Iron-Iron Carbide Nanocrystalline Particles by Using Power Ultrasound. *Angew. Chem. Int. Ed.* **2001**, *40*, 4447-4449.

(18) Geng, J.; Jefferson, D. A.; Johnson, B.F.G. Direct Conversion of Iron Stearate into Magnetic Fe and Fe_3C Nanocrystals Encapsulated in Polyhedral Graphite Cages. *Chem. Commun.* **2004**, 2442-2443.

(19) Lu, A.-H.; Li, W.-C.; Matoussevitch, N.; Spliethoff, B.; Bönneman, H.; Schüth, F. Highly Stable Carbon-Protected Cobalt Nanoparticles and Graphite Shells. *Chem. Commun.* **2005**, 98-100.

(20) Zalich, M. A.; Baranauskas, V. V.; Riffle, J. S.; Saunders, M.; St Pierre, T. G. Structural and Magnetic Properties of Oxidatively Stable Cobalt Nanoparticles Encapsulated in Graphite Shells. *Chem. Mater.* **2006**, *18*, 2648-2655.

(21) Zhu, G.-X.; Wei, X.-W.; Xia, C.-J.; Ye, Y. Solution Route to Single Crystalline Dendritic Cobalt Nanostructures Coated with Carbon Shells. *Carbon* **2007**, *45*, 1160-1166.

(22) Zadoina, L.; Soulantica, K.; Ferrere, S.; Lonetti, B.; Respaud, M.; Mingotaud, A.-F.; Falqui, A.; Genovese, A.; Chaudret, B.; Mauzac, M. In Situ Synthesis of Cobalt Nanoparticles in Functionalized Liquid Crystalline Polymers. *J. Mater. Chem.* **2011**, *21*, 6988- 6994.

(23) Schrittwieser, S.; Ludwig, F.; Dieckhoff, J.; Soulantica, K.; Viau, G.; Lacroix, L.-M.; Mozo Lentijo, S.; Boubekri, R.; Maynadié, J.; Huetten, A.; Brueckl, H.; Schotter, J. Modeling

and Development of a Biosensor Based on Optical Relaxation Measurements of Hybrid Nanoparticles. *ACS Nano* **2012**, *6*, 791-801.

(24) Soumare, Y.; Garcia, C.; Maurer, T.; Chaboussant, G.; Ott, F.; Fiévet, F.; Piquemal, J.-Y.; Viau, G. Kinetically Controlled Synthesis of Cobalt Nanorods with High Magnetic Coercivity. *Adv. Funct. Mater.* **2009**, *19*, 1971-1977.

(25) Soulantica, K.; Wetz, F.; Maynadie, J.; Falqui, A.; Tan, R. P.; Blon, T.; Chaudret, B.; Respaud, M. Magnetism of single-crystalline Co nanorods. *Appl. Phys. Lett.* **2009**, *95*, 152504.

(26) Maurer, T. ; Ott, F. ; Chaboussant, G. ; Soumare, Y. ; Piquemal, J.-Y. ; Viau, G. Magnetic Nanowires as Permanent Magnet Materials. *Appl. Phys. Lett.,* **2007**, *91*, 172501.

(27) Ait Atmane, K. ; Zighem, F. ; Soumare, Y. ; Ibrahim, M. ; Boubekri, R. ; Maurer, T. ; Margueritat, J. ; Piquemal, J.-Y. ; Ott, F. ; Chaboussant, G. ; Schoenstein, F. ; Jouini, N. ; Viau, G. High Temperature Structural and Magnetic Properties of Cobalt Nanorods. *J. Solid State Chem.,* **2013**, *197*, 297.

[28] Sutter, E.; Sutter, P. Au-Induced Encapsulation of Ge Nanowires in Protective C Shells. *Adv. Mater.* **2006**, *18*, 2583-2588.

(29) Zickler, G. A.; Smarsly, B.; Gierlinger, N.; Peterlik, H.; Paris, O. A Reconsideration of The Relationship Between The Crystallite Size L_a of Carbons Determined by X-Ray Diffraction and Raman Spectroscopy. *Carbon* **2006**, *44*, 3239–3246.

(30) NIST X-ray Photoelectron Spectroscopy Database; data compiled and evaluated by Wagner, C. D.; Naumkin, A. V.; Kraut-Vass, A.; Allison, J. W.; Powell, C. J.; Rumble, J. R. http://srdata.nist.gov/xps/

[31] Maurer, T.; Zighem, F.; Ott, F.; Chaboussant, G.; André, G.; Soumare, Y.; Piquemal, J.-Y.; Viau, G.; Gatel, C. Exchange Bias in *Co/CoO* Core-Shell Nanowires: Role of The Antiferromagnetic Superparamagnetic Fluctuations. *Phys. Rev.* B **2009**, *80*, 064427.

(32) JCPDS reference powder diffraction file 01-072-1369

(33) Harris, V. G.; Chen, Y.; Yang, A.; Yoon, S.; Chen, Z.; Geiler, A. L.; Gao, J.; Chinnasamy, C. N.; Lewis, L. H.; Vittoria, C.; Carpenter, E. E.; Carroll, K. J.; Goswami, R.; Willard, M. A.; Kurihara, L.; Gjoka, M.; Kalogirou, O. High Coercivity Cobalt Carbide Nanoparticles Processed Via Polyol Reaction: A New Permanent Magnet Material. *J. Phys.* D : *Appl. Phys.* **2010**, *43*, 165003.

(34) Zhang, Y.; Chaubey, G. S.; Rong, C.; Ding, Y.; Poudyal, N.; Tsai, P.-C.; Zhang, Q.; Ping Liu, J. Controlled Synthesis and Magnetic Properties of Hard Magnetic Co_xC (x=2, 3) Nanocrystals. *J. Magn. Magn. Mater.* **2011**, *323*, 1495-1500.

(35) Caroll, K. J.; Huba, Z. J.; Spurgeon, S. R.; Qian, M.; Khanna, S. N.; Hudgins, D. M.; Mitra, M. L.; Carpenter, E. E. Magnetic Properties of Co_2C and Co_3C Nanoparticles and their Assemblies. *Appl. Phys. Lett.* **2012**, *101*, 012409.

(36) Nagakura, S. Study of Metallic Carbides by Electron Diffraction Part IV. Cobalt Carbides *J. Phys. Soc. Jpn.* 1961, *16*, 1213.

(37) Tan, K. F.; Xu, J.; Chang, J.; Borgna, A.; Saeys, M. Carbon Deposition on Co Catalysts during Fischer–Tropsch Synthesis: A Computational and Experimental Study. *J. Catal.* **2010**, *274*, 121-129.

(38) Ducreux, O.; Rebours, B.; Lynch, J.; Roy-Auberger, M.; Bazin D. Microstructure of Supported Cobalt Fischer-Tropsch Catalysts. *Oil & Gas Science and Technology – Rev. IFP,* **2009**, *64*, 49-62.

FIGURE CAPTIONS

Figure 1 Raman spectra of cobalt nanowires treated in an organic solvent at 300 °C for 3h : (a) octadecene $I_D/I_G = 0.67$; (b) oleylamine $I_D/I_G = 0.80$.

Figure 2 (a) SEM, (b) TEM and (c) HRTEM images of cobalt rods coated with a thin carbon shell by a treatment in ODE at 300 °C for 3h (the circles indicate local onion structure with a distance in the range 3.4-3.5 Å).

Figure 3 X-ray photon electron spectra of cobalt rods and cobalt rods coated by a thin carbon shell by a treatment in ODE at 300 °C for 3h: (a) survey scans ; (b) Peak fitting of Co 2p peak high resolution scans.

Figure 4 XRD pattern of Co rods treated (a) in ODE for 3h and in a mixture of ODE/OA for (b) 30 min, (c) 3h and (d) 4h (only the Co_2C strongest lines are indexed).

Figure 5 TEM images of cobalt rods treated at 300 °C (a) for 3h in OA and (b) for 4h in a mixture ODE/OA.

Figure 6 HRTEM image of a cobalt rod treated in an ODE/OA mixture at 300 °C for 3h. Numerical diffraction patterns of the two different zones as inset.

Figure 7 In-situ X-ray diffraction patterns under N_2 ($O_2 < 2$ ppm) of (a) carbon coated Co nanorods and (b) non coated Co nanorods; (c) Variation of the $L_{(10\bar{1}0)}$ and $L_{(0002)}$ mean crystallite sizes with increasing temperature of the carbon coated Co nanorods.

Figure 8 In situ X-ray diffraction patterns of carbon coated and partially carburized Co nanorods annealed under N_2 ($O_2 < 0.1$ ppm).

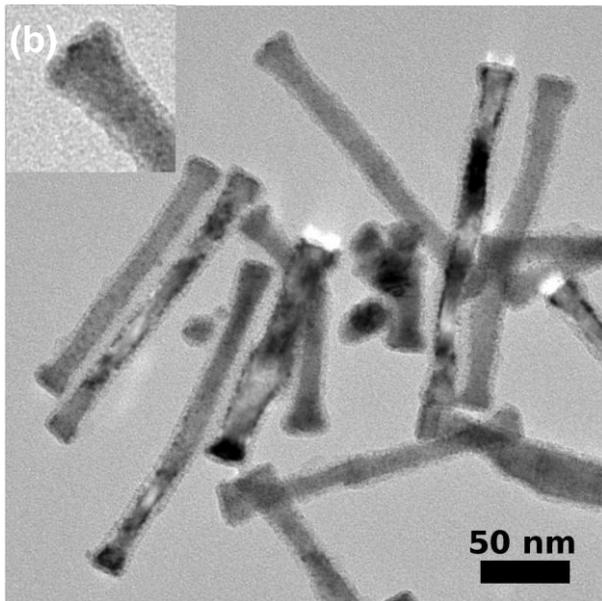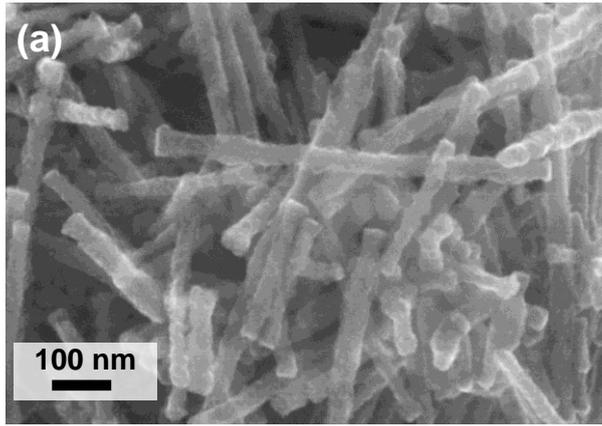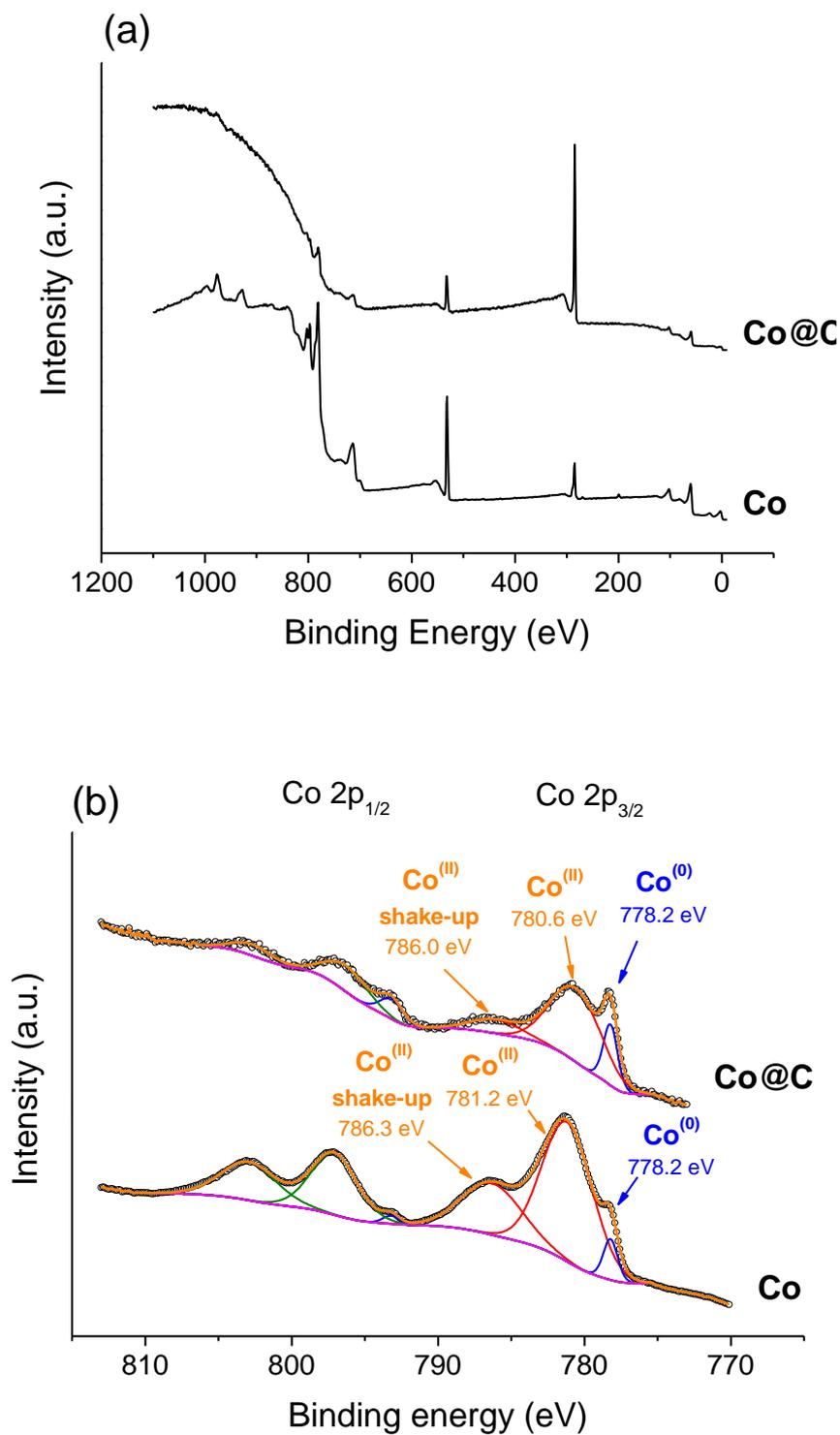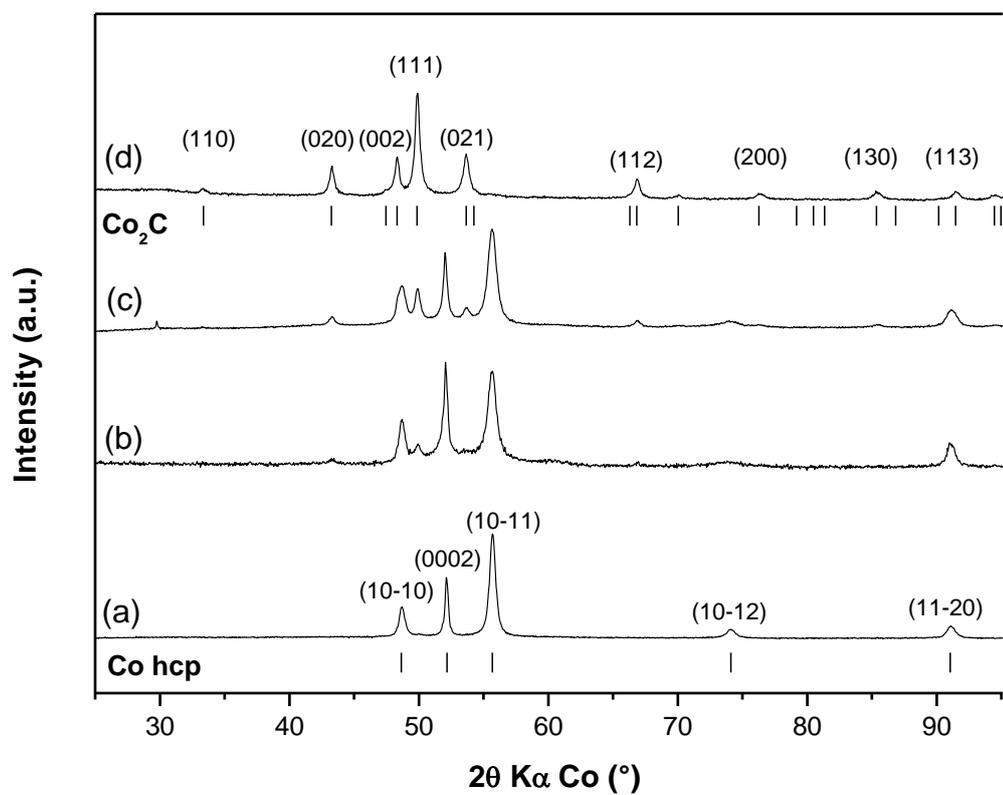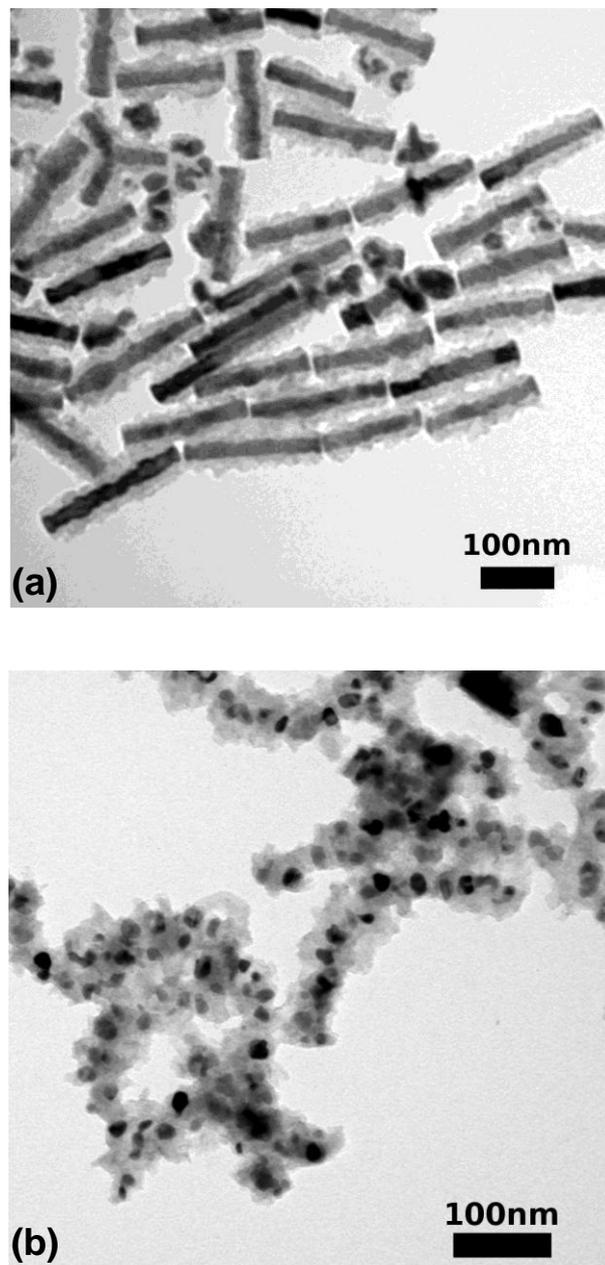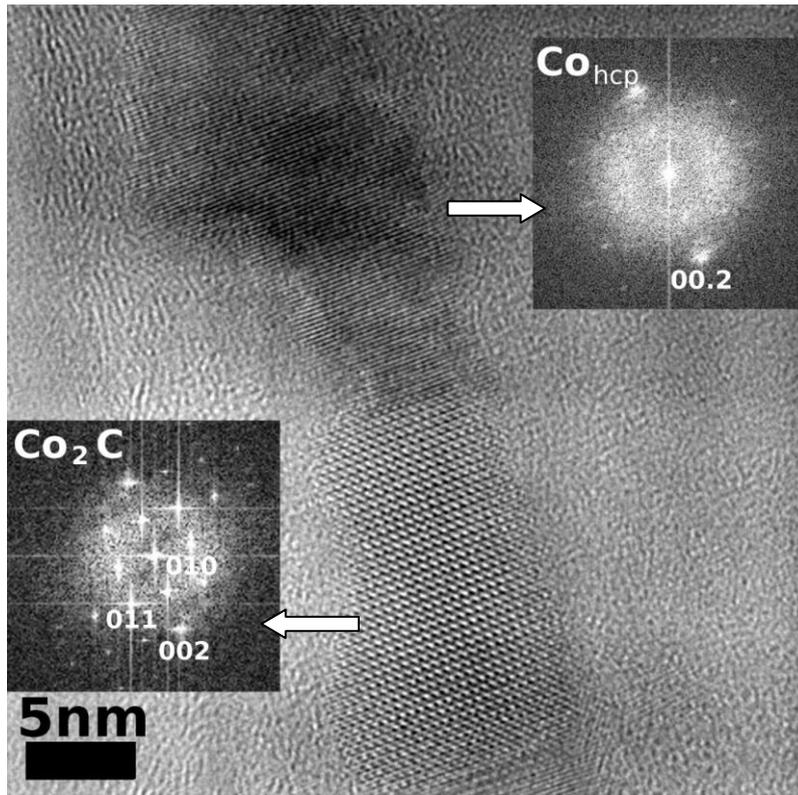**Figure 9** TEM image of carbon coated Co nanorods annealed at 400 °C under N_2 ($O_2 < 0.1$ ppm) for 2h.

Figure 10 Room temperature magnetization curve of carbon coated Co nanorods (black) and of the same coated rods annealed at 400 °C under N_2 ($O_2 < 0.1$ ppm) for 2h (red).

Figure 11 Scheme of formation of a Co_2C grain in a cobalt rod by intercalation of C atoms from the $(10\bar{1}0)$ sides of the hcp Co.

Figure 1 Raman spectra of cobalt nanowires treated in an organic solvent at 300 °C for 3h :
(a) octadecene $I_D/I_G = 0.67$; (b) oleylamine $I_D/I_G = 0.80$.

Figure 2 (a) SEM, (b) TEM and (c) HRTEM images of cobalt rods coated with a thin carbon shell by a treatment in ODE at 300 °C for 3h (the circles indicate local onion structure with a distance in the range 3.4-3.5 Å).

Figure 3 X-ray photon electron spectra of cobalt rods and cobalt rods coated by a thin carbon shell by a treatment in ODE at 300°C for 3h: (a) survey scans ; (b) Peak fitting of Co 2p peak high resolution scans.
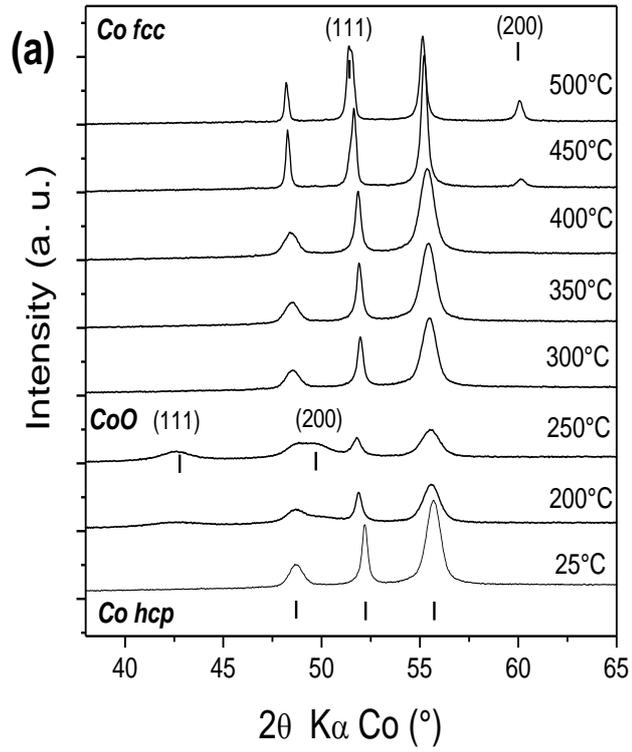
Figure 4 XRD pattern of Co rods treated (a) in ODE for 3h and in a mixture of ODE/OA for (b) 30 min, (c) 3h and (d) 4h (only the Co_2C strongest lines are indexed).
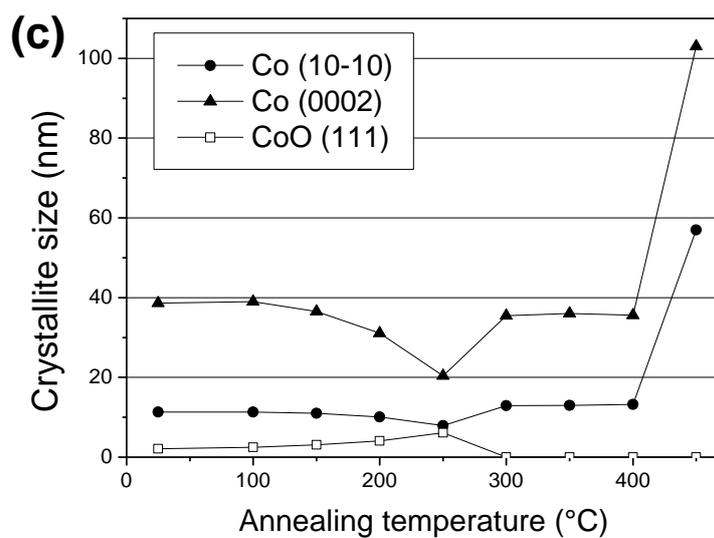
Figure 5. TEM images of cobalt rods treated at 300 °C (a) for 3h in OA and (b) for 4h in a mixture ODE/OA.
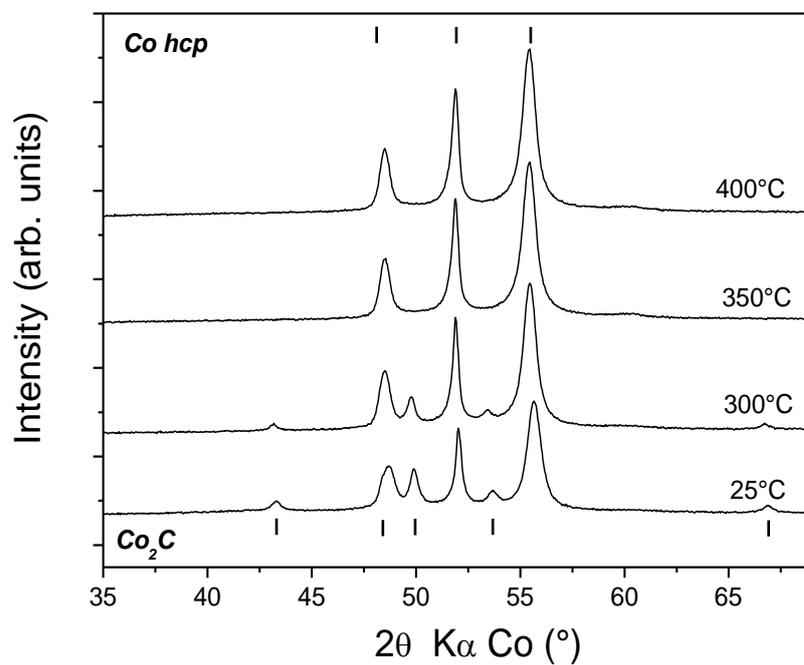
Figure 6 HRTEM image of a cobalt rod treated in an ODE/OA mixture at 300 °C for 3h. Numerical diffraction patterns of the two different zones as inset.
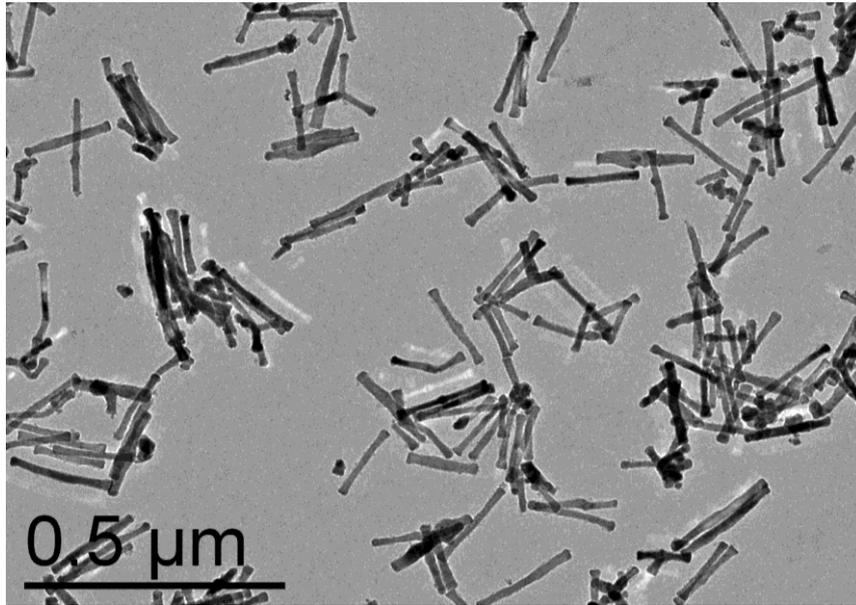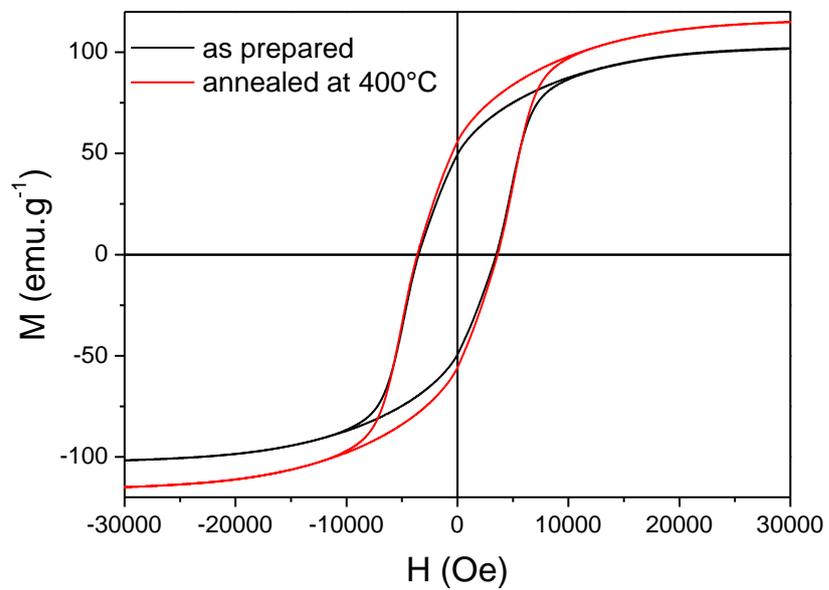
(a)

Co fcc

(111) (200)

500°C
450°C
400°C
350°C
300°C

CoO (111) (200)

250°C
200°C
25°C

Co hcp

Intensity (a. u.)

2θ Kα Co (°)

40 45 50 55 60 65

(b)

Co

(311) CoO

(220) Co Co

(222) 350°C

(400) (422) (511) (440)

Co₃O₄

300°C

250°C

200°C

CoO (111) (200) (220)

25°C

Co hcp

Intensity (arb. units)

30 40 50 60 70 80

Figure 7 In-situ X-ray diffraction patterns under N_2 ($O_2 < 2$ ppm) of (a) carbon coated Co nanorods and (b) non coated Co nanorods; (c) Variation of the $L_{(10\bar{1}0)}$ and $L_{(0002)}$ mean crystallite sizes with increasing temperature of the carbon coated Co nanorods.
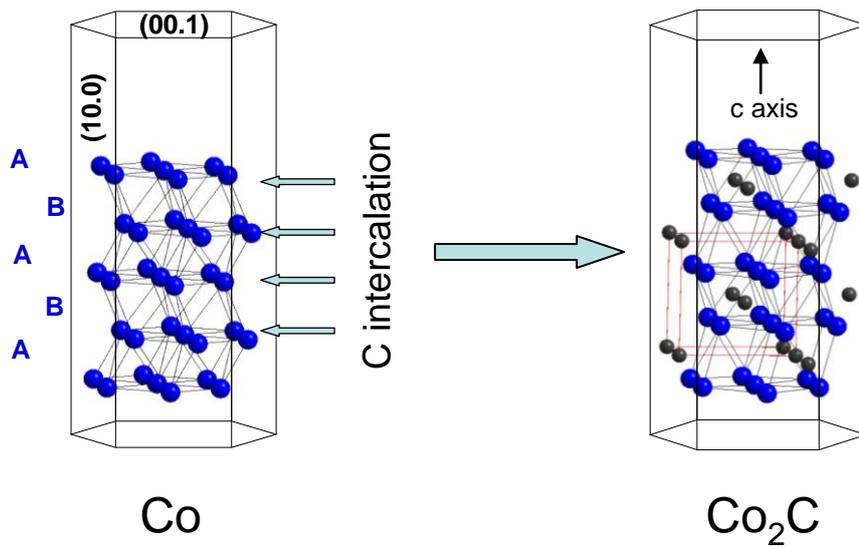
Figure 8 In situ X-ray diffraction patterns of carbon coated and partially carburized Co nanorods annealed under N_2 ($O_2 < 0.1$ ppm).

Figure 9 TEM image of carbon coated Co nanorods annealed at 400 °C under N_2 ($O_2 < 0.1$ ppm) for 2h.

Figure 10. Room temperature magnetization curve of carbon coated Co nanorods (black) and of the same coated rods annealed at 400 °C under N_2 ($O_2 < 0.1$ ppm) for 2h (red).

Figure 11. Scheme of formation of a Co_2C grain in a cobalt rod by intercalation of C atoms from the $(10\bar{1}0)$ sides of the hcp Co.

Graphical Abstract

Carbon Coating, Carburization and High Temperature Stability Improvement of Cobalt Nanorods

Mona Ibrahim, Cécile Garcia, Kahina Ait Atmane, Ekrame Berrichi, Antoine Zwick, Bénédicte Warot-Fonrose, Lise-Marie Lacroix, Sébastien Lachaize, Phillipe Decorse, Jean-Yves Piquemal and Guillaume Viau